13

Growth of CZTS-Based Monograins and Their Application to Membrane Solar Cells

Enn Mellikov, Mare Altosaar, Marit Kauk-Kuusik, Kristi Timmo, Dieter Meissner, Maarja Grossberg, Jüri Krustok and Olga Volobujeva

Department of Materials Science, Tallinn University of Technology, Ehitajate tee 5, 19086 Tallinn, Estonia

13.1 Introduction

The idea of producing solar cells from powder materials is nearly as old as the history of modern silicon-based solar cells. Just three years after AT&T Bell Lab's Chapin, Fuller, and Pearson released their first commercially attractive silicon solar cell [1], Hoffman's Electronics patented a method to produce solar modules from silicon powders [2]. Based on Hoffman's Electronics' patents, Ties Siebold te Velde of Philips Company in Eindhoven filed the first patent on monograin membrane devices for radiation detection, use in a solar battery, a LED, etc. [3]. Eighteen further patents had been filed by 1973, specifying methods of membrane production as well as new applications such as the production of printed circuits. Philips continued to produce monograin membrane-based photoconductive elements containing 35–45 μm Cu-doped CdS particles in Hamburg until the mid-1990s. Meanwhile, in the mid-1970s the technology to produce silicon spheres and insert these into an aluminum foil with appropriately placed holes had been developed at Texas Instruments in order to electrolyze a solution to store light energy as chemical energy in electrolysis products [4].

Copper Zinc Tin Sulfide-Based Thin-Film Solar Cells, First Edition. Edited by K. Ito.

Following this first patent, several more were filed at the beginning of the 1990s. In 1985, Texas Instruments in cooperation with the Southern California Edison Company (SCE) started to develop a Spheral Solar Cell using metallurgical silicon of low purity. This device, represented by more than 40 worldwide patents, comprises tiny silicon spheres bonded between thin flexible aluminum foil substrates to form solar cells, which are then assembled into durable, lightweight modules that can be applied to virtually any surface. Kyosemi Corporation, Japan has developed Sphelar, a spherical solar-cell technology that captures sunlight in three dimensions. The technology is based on an array of single-crystalline silicon spheres, each measuring 1–2 mm across, embedded in a transparent medium. Each sphere functions as an individual, miniature solar cell [5]. Further historical background of powder-based solar cell applications can be found in [6].

Research and development of monograin-layer (MGL) solar cells at Tallinn University of Technology (TUT) began in 1996 after a two-year period of inquiry in the field of $CuInSe_2$ monograin powder growth. Monograin is a single-crystalline powder particle consisting of one single crystal or several single-crystalline blocks grown into a compact grain. The cross-section of the MGL solar cell is depicted in Figure 13.1a. The MGL solar cells have a superstrate structure of graphite/MGL/CdS/ZnO/glass, where the monograin layer is a monolayer of powder grains embedded into an organic resin so that the upper part of the grains remains uncovered. CdS is deposited on top of the MGL (or onto the surface of the monograins before MGL formation) by chemical bath deposition, followed by RF-sputtering of i-ZnO and conductive ZnO:Al layers. Finally, highly conductive grid contacts are evaporated on top of the ZnO window layer, and the structure is glued onto a glass or some other durable transparent substrate. For back conducting, the bottom side of the MGL is polished to remove polymer from powder crystals and to expose monograins before applying graphite contacts. Our group of authors began conducting research to create and commercialize modules of powder-based $Cu_2ZnSn(S_xSe_{1-x})_4$ (CZTSSe) MGL solar cells in 2008 and has continued in collaboration with the TUT spin-off company *crystalsol OÜ*. A pilot production line is set up in the research and development facility of *crystalsol GmbH* in Austria.

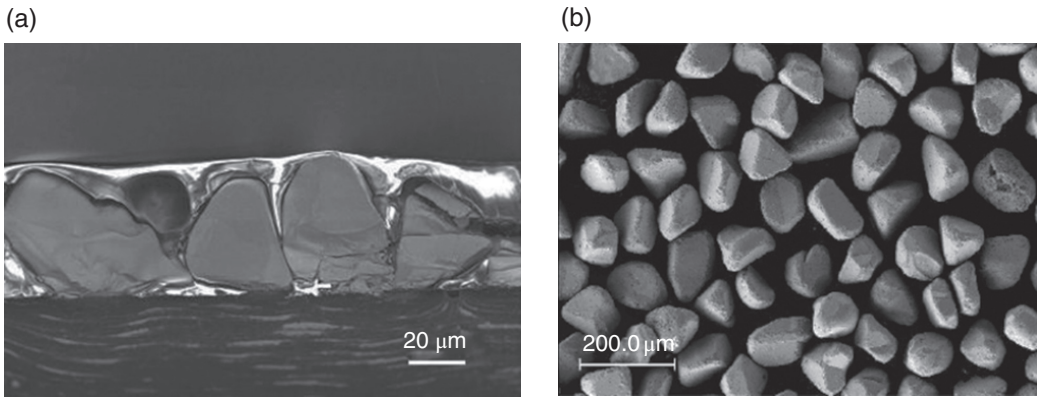

Figure 13.1 *(a) Cross-section of monograin layer solar cell structure; and (b) SEM micrograph of a $Cu_2ZnSn(S,Se)_4$ monograin powder synthesized in KI flux (size fraction 90–100 μm)*

The MGLs combine the high photoelectrical parameters of single crystals and the advantages of polycrystalline materials and technologies, that is, low cost and simple technology of materials and devices, and the possibility of making flexible devices and using the materials up to 100%. MGL technology allows the separation of materials formation from module fabrication. Large-area modules are fabricated at room temperature in a continuous roll-to-roll process. Homogeneous composition of powders gives an additional advantage, leading to homogeneous modules without any up-scaling problem.

13.2 Monograin Powder Growths, Basics of the Process

Molten salts have proven to be useful as alternative reaction media for various organic and inorganic reactions [7, 8]. Single crystals or single-crystalline powders can be obtained at temperatures above the melting point of the used salt at temperatures lower than the melting point of the semiconductor itself. Synthesis in molten salts enhances the rate of solid-state reactions due to the much higher diffusion rates between reaction components in the molten media [9], lowering the reaction temperature, increasing the homogeneity of the solid product, and controlling the particle size and shape as well as their agglomeration state.

In the material formation-nucleation stage, the precursors: (1) can dissolve completely in the molten salt, with the nuclei of the product formed in the liquid phase (growth of single crystals); or (2) initial solid particles of low-solubility precursors react with each other in the molten salt media, and the formed solid particles of the product compound start to recrystallize and grow by the mechanism of Ostwald ripening [10] (monograin powder growth). In the growth of monograin powders, the crystals are formed in the presence of the liquid phase of the used flux salt. The characteristics of monograin powder crystals are controlled by selection of the synthesis temperature, as well as the nature and amount of the salt. The volume of the used molten salt has to exceed the volume of voids between precursor particles. In this case the formed liquid phase is sufficient to repel both the solid precursor particles and the formed powder particles from each other and to avoid sintering caused by the contracting capillary forces arising in the solid–liquid phase boundaries. The amounts of precursors for CZTSSe and flux salt are therefore usually taken so that the ratio of the forming volumes of solid phase V_S and liquid phase V_L is within the range 0.6–1.0 [11]. After the synthesis, the used salt is removed by washing with a suitable solvent and the released monograin powder is dried and sieved (Fig. 13.1b).

Research on II–VI compounds monograin powder growth in Na_2S_x and $CdCl_2$ was initiated at Tallinn University of Technology in the 1970s and the research into $CuInSe_2$ monograin powders in the 1990s [11]. During the first investigations, Se, CuSe, and mixtures of Se-CuSe were used as flux materials for $CuInSe_2$ [12–14] and Te or $CdCl_2$ for CdTe monograin production [15, 16]. Although monograins with nearly stoichiometric $CuInSe_2$ composition were obtained using CuSe-Se as a flux, the removal of the flux material after the synthesis was difficult; CuSe-Se was therefore soon replaced by water-soluble potassium iodide (KI) [17]. KI has low hygroscopicity and also low solubility in $CuInSe_2$. Since 2006, research and development of monograin powder technology has mainly been directed to $Cu_2ZnSnSe_4$, Cu_2ZnSnS_4, and their solid solutions [18, 19]. KI, NaI, and CdI_2, with their low melting point, low vapor pressure, and high solubility in water, were used as flux materials [20–22].

13.2.1 Chemical Pathway of $Cu_2ZnSnSe_4$ Formation in the Presence of Flux Salts

The pathway of $Cu_2ZnSnSe_4$ formation from binary chalcogenides (ZnSe, CuSe, and SnSe) in KI, NaI, and CdI_2 was studied by DTA, micro-Raman, XRD, SEM, and EDX methods [20–22]. DTA, XRD and Raman analyses confirm that the formation of a liquid phase is the initiator of chemical reactions; CZTSe can be recognized at 380°C after the melting of Se that results from the transformation of CuSe to $Cu_{2-x}Se$ and Se. In the presence of solid salt, the CZTSe formation process is then impeded to a great extent until the flux salt melts. The melting is immediately followed by the extensive exothermic process of CZTSe formation. The chemical pathway begins after the release of Se from CuSe at the peritectic phase transformation temperature (380°C [20–22]) of CuSe to $Cu_{2-x}Se$ + Se in all the precursor-flux mixtures studied. Se then reacts with SnSe resulting in $SnSe_2$, and $Cu_{2-x}Se$ reacting with $SnSe_2$ then forms Cu_2SnSe_3. The reaction of Cu_2SnSe_3 with ZnSe ends the chemical route of CZTSe formation. Before the formation of the liquid phase of flux, the resultant amounts of formed CZTSe and Cu_2SnSe_3 are low and the reflections of unreacted phases of $Cu_{1.8}Se$, CuSe, ZnSe, SnSe, and $SnSe_2$ are present in the XRD patterns of samples heated at temperatures below the melting temperature of the used salt. The CZTSe formation reactions before the formation of liquid phase of flux are probably inhibited due to a number of different factors. First, the formed Se overpressure in the closed vacuum ampoules suppresses the further decomposition of CuSe and therefore also the supply of Se. Second, the large amount of solid NaI between solid particles of precursors inhibits the diffusion rate of reaction components and, due to this, the rate of CZTSe formation is also suppressed.

The use of CdI_2 as flux results in the formation of $Zn_{1-x}Cd_xSe$ solid solution as an intermediate product and $Cu_2(Zn_{1-x}Cd_x)SnSe_4$ as a final product, in which the amount of incorporated Cd changes from 1.3 to 3 at% depending on the synthesis temperature used. In the studies of CZTSe formation in NaI, the specific enthalpy of exothermic $Cu_2ZnSnSe_4$ formation –36 ± 3 kJ/mol was determined experimentally. The formation of ternary compound Na_2SnSe_3 was detected during the synthesis process in NaI. If present in NaI, $NaI{\cdot}2H_2O$ was found to be a critical issue in the synthesis process of CZTSe monograin powders in molten NaI, as it gave rise to the formation of oxygen-containing by-products Na_2SeO_4 and $Na_2Cu(OH)_4$. The complete dehydration of $NaI{\cdot}2H_2O$ at $T \leq 70$°C in vacuum is necessary to avoid the formation of oxygen-containing compounds.

As the CZTSe monograin powder crystals grow in molten KI, they saturate with K and I. The solubility of K in CZTSe is determined by ICP-MS as 5.5×10^{17} at cm^{-3}.

13.2.2 Elemental and Phase Compositions of CZTS-Based Monograins

It has been found that the crystal growth of single-phase CZTS with Cu-poor and Zn-rich composition is a prerequisite for improving the efficiency of kesterite thin-film solar cells. Cu-poor conditions enhance the formation of Cu vacancies, which gives rise to shallow acceptors in CZTS, while Zn-rich conditions suppress the substitution of Cu at Zn sites, which gives rise to relatively deep acceptors [23]. It is therefore very important to determine the composition and compositional limits of formation of single-phase kesterite powders and to control these parameters in the powder growth process. One of the main tools for controlling parameters and phase structure of CZTS and CZTSe monograin powders is

changing the initial precursor composition [24, 25]. Compositional variations of precursors and product material are ordinarily expressed by two parameters: [Cu]/([Zn]+[Sn]) and [Zn]/[Sn], where [Cu], [Zn], and [Sn] are atomic concentrations (at%) of elements in the bulk of powder crystals.

13.2.2.1 Cu_2ZnSnS_4

Figure 13.2 gives the values of compositional ratios Cu/(Zn+Sn) and Zn/Sn of the synthesized CZTS monograins depending on the composition of precursors.

In slightly Zn-rich conditions (Zn/Sn=1.03), the increase in the ratio of [Cu]/([Zn]+[Sn]) in the precursor mixture decreased the ratio of [Zn]/[Sn] from 1.03 to 0.92 in the final product (see Fig. 13.2a). When the ratio of [Cu]/([Zn]+[Sn]) in precursors was increased to over 0.95, the powder composition became Sn-rich in addition to Cu-rich. It was found that, in these growth conditions, secondary phases such as Cu- and Sn-binaries and Cu_2SnS_3 were formed together with quaternary compound.

In Zn-rich growth conditions ($1.03<Zn/Sn\leq1.2$) with constant Cu content in precursors (Fig. 13.2b), the composition of formed CZTS powder crystals was invariable. Only an amount of ZnS secondary phase was increased by the addition of Zn in the precursors' mixture.

In Zn-poor growth conditions ($Zn/Sn<1.0$) with constant Cu content in precursors, the composition of CZTS powder crystals became Cu-rich and Sn-rich. In the case of the highest Cu content in the precursors (Cu/(Zn+Sn)=1.1), additional phases of SnS, SnS_2, and Sn_2S_3 were detected by Raman and EDX analysis.

SEM images of polished CZTS crystals are shown in Figure 13.3a and b. The formation of a separate phase of $Cu_{2-x}S$ in powders with an excess of Cu is in agreement with the phase diagram assembled by Olekseyuk *et al.* [26]. The SEM, EDX and Raman

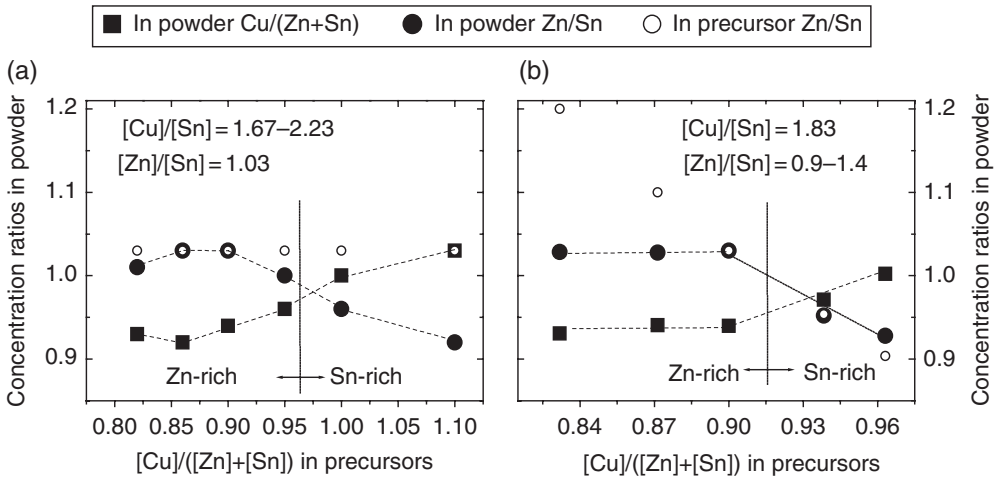

Figure 13.2 *[Cu]/([Zn]+[Sn]) (filled squares) and [Zn]/[Sn] (filled dots) ratios of Cu_2ZnSnS_4 monograin powders determined by EDX as a function of the [Cu]/([Zn]+[Sn]) ratio in precursors when (a) [Zn]/[Sn] was kept constant and (b) [Cu]/[Sn] was kept constant. Hollow dots represent the Zn to Sn concentration ratio in precursors. Reproduced from [24]. With permission from Elsevier*

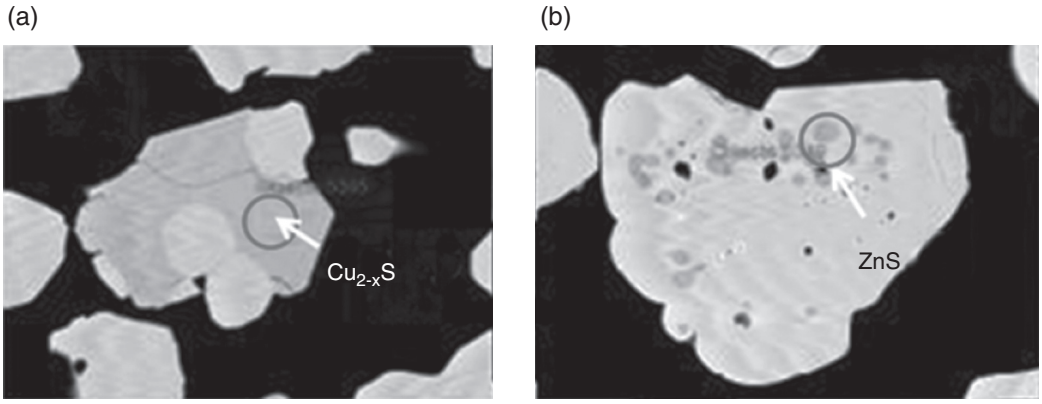

Figure 13.3 *SEM images of mechanically polished (a) Cu-rich and (b) Zn-rich CZTS crystals, indicating the existence of different separate binary phases in monograins. Reproduced from [24]. With permission from Elsevier*

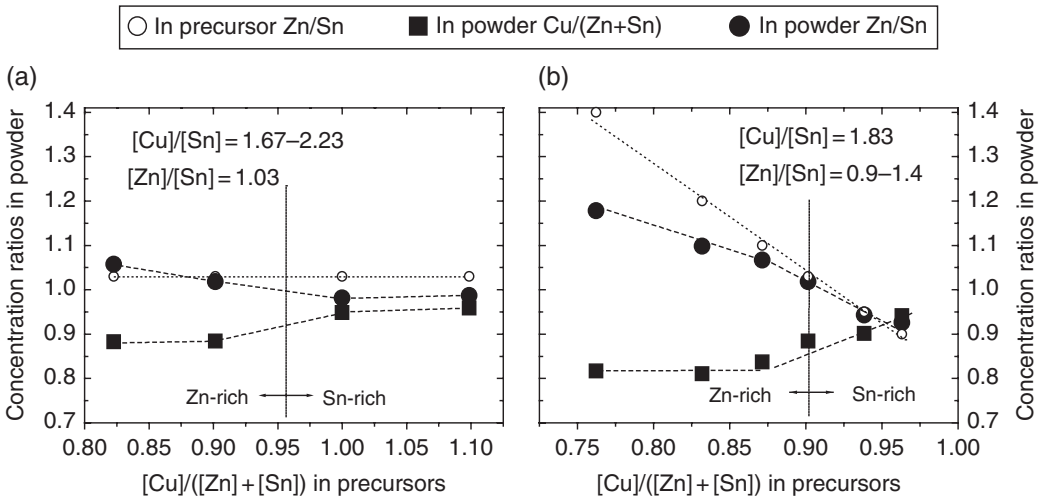

Figure 13.4 *[Cu]/([Zn]+[Sn]) (filled squares) and [Zn]/[Sn] (filled dots) ratios of $Cu_2ZnSnSe_4$ monograin powders depending on the [Cu]/([Zn]+[Sn]) ratio in precursors if (a) [Zn]/[Sn]=1.03 and (b) [Cu]/[Sn]=1.83. Hollow dots represent the Zn/Sn concentration ratio in precursors. Reproduced from [25]. With permission from Elsevier*

investigations showed that powders with initial compositional ratio of Cu/(Zn+Sn) below 0.95 and Zn/Sn>1.03 contain a separate phase of ZnS.

13.2.2.2 $Cu_2ZnSnSe_4$

Similar investigations to those presented in the previous section were made with a $Cu_2ZnSnSe_4$ system. Several powders with different Cu and Zn content in precursors were grown to study the influence of precursor composition on the Cu and Zn content in CZTSe monograin powders [25]. The metal composition ratios of the initial (hollow dots) and synthesized (filled squares and dots) monograins are shown in Figure 13.4a and b.

In slightly Zn-rich growth conditions (Zn/Sn=1.03), the increase in the ratio of [Cu]/([Zn]+[Sn]) in the precursor mixture decreased the ratio of Zn/Sn in the final product from 1.03 to 0.98 (see Fig. 13.4a). The deviation from precursor composition is much smaller than in the sulfide system. When the compositional ratio of Cu/(Zn+Sn) in precursors was increased to >1.0, the powder composition also became slightly Sn-rich in addition to being Cu-rich. In the latter growth conditions, Cu_xSe and $SnSe_2$ secondary phases were detected by Raman analysis.

In highly Zn-rich conditions (Zn/Sn = 1.1–1.4) with constant Cu/Sn ratio in precursors, the CZTSe powder crystals had a stable Cu/(Zn+Sn) compositional ratio of about 0.81. Only the presence of ZnSe secondary phase was always detected in these powder crystals by Raman spectroscopy. In the sulfide system, the compositional ratio of Cu/(Zn+Sn) in monograin powders was much higher (0.94).

When we compare a Cu_2ZnSnS_4 system with a $Cu_2ZnSnSe_4$ system, the existence of a composition region for the synthesis of single-phase quaternary monograins extends toward the pure selenide and is mainly regulated by Cu and Zn content in precursors. Cu and Zn content in the synthesized material are interchangeable to some extent: higher copper content in the initial precursors is always accompanied by lower Zn content in the product material and vice versa.

13.3 Influence of Chemical Etching on the Surface Composition of Monograins

The solubility of CZTSe in KI is 0.6 mole% for CZTSe, while those of CuSe, ZnSe, and SnSe are 3.6, 0.09, and 0.3 mole%, respectively, at 740°C [21]. This means that at high temperatures, a part of the precursors and the synthesized kesterite dissolves in the flux. During cooling from a growth temperature, some part of the dissolved precursors and CZTSe precipitate on the surface of the monograins; the surface composition of crystals therefore depends on their precipitations. The EDS analysis revealed that the surface composition of as-grown crystals was Sn-rich while the bulk of monograins was Zn-rich. In addition, it was confirmed by XPS analysis that the surface of monograins exhibits Cu deficiency and an excess of Sn and chalcogens (Fig. 13.5). The [Zn]/[Sn] (Fig. 13.6) changes from 0.88 at the surface to 1.06 in the bulk and the [Cu]/([Zn]+[Sn]) increases from 0.63 at the surface to 0.92 in the bulk.

Chemical treatments with several etchants (HCl, KCN, Bromine in methanol (Br_2-MeOH) and NH_4OH) were performed in order to improve the active interface of solar cells [27]. Polarographic analysis of the leaching solutions indicated that preferably Sn and chalcogen were removed from the surface by HCl etching, probably due to the complexation of Sn in HCl solution and formation of $[SnCl_4]^{2-}$ [28]. The KCN etching is well known as a process to remove Cu-Se binary phases [29], but we also detected Sn in the leaching solutions. The ammonia solution selectively removed Cu and chalcogen from the surface.

Figure 13.7 represents XPS spectra of the as-grown and Br_2-MeOH-etched $Cu_2ZnSn(S,Se)_4$ monograin surfaces. The intensity of Cu2p, CuLMM peaks decreases and the intensity of the Sn and O1s peaks increases after etching materials with Br_2-MeOH. Zn2p and ZnLMM peaks are almost undetectable for materials etched with Br_2-MeOH.

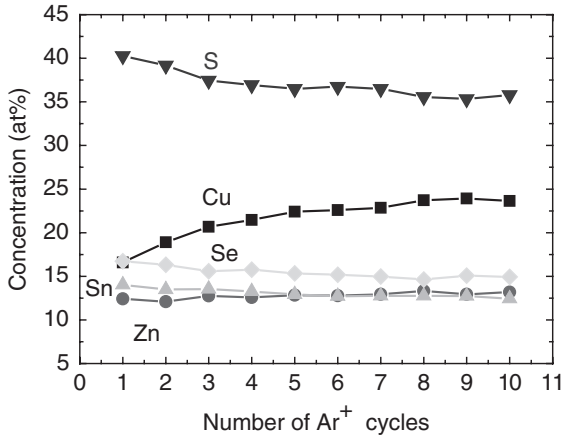

Figure 13.5 *XPS depth profiling of element concentrations of CZTSSe monograin powder crystal surface*

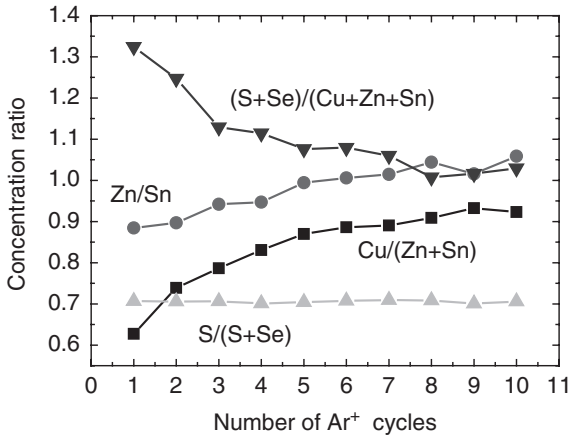

Figure 13.6 *Concentration ratios of elements of CZTSSe monograin powder crystal surface*

The relative atomic concentrations of Zn, Cu, Sn, and Se were determined from integrated peak areas of high-resolution XPS core level spectra. The S2p peak area was determined by core level curve-fitting procedures since this peak overlaps with the Se3p core level. The composition of the $Cu_2ZnSn(S,Se)_4$ monograin surface etched in the Br_2-MeOH solution was determined by XPS with the following result: Cu : Zn : Sn : S+Se : O = 1.2 : 1.2 : 37.0 : 12.8 : 47.7 at%. Comparison of the XPS spectra of the as-grown and the Br_2-MeOH-etched samples allows us to conclude that Br_2-MeOH-etching mainly removes Cu and Zn. This fits well with the results of the polarographic analysis of the leaching solutions (Table 13.1).

Solar cell parameters made from chemically treated $Cu_2ZnSn(S_{0.45}Se_{0.55})_4$ monograin powders are given in Table 13.2. All the etched powders were post-annealed in the isothermal conditions in closed ampoules at 740°C before fabricating MGL solar cells.

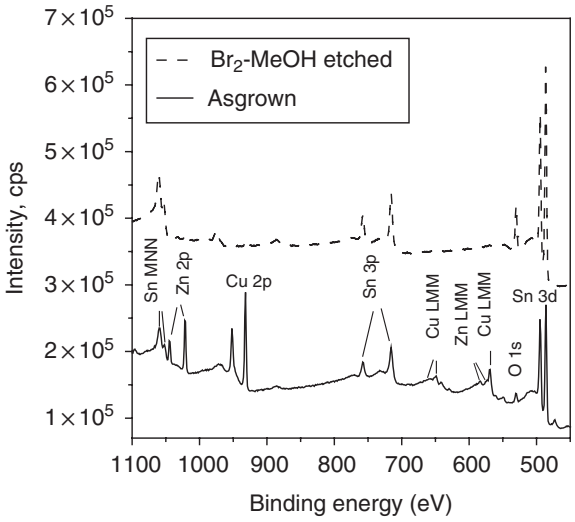

Figure 13.7 *XPS spectra of surfaces of the as-grown and Br_2-MeOH etched CZTSSe monograins*

Table 13.1 *Molar ratios of elements in leaching solutions determined polaro-graphically [28]*

Etchant/element	Cu: Zn: Sn: Se
KCN	1.0 : 0 : 0.4 : 1.5
HCl	1.0 : 0.1 : 5.8 : 6.5
NH_4OH	1.0 : 0.2 : 0 : 2.2
Br_2-MeOH	1.0 : 0.8 : 0.7 : 0.3

Table 13.2 *Performance parameters (open-circuit voltage V_{oc}, short-circuit current density J_{sc}, fill factor FF, solar cell efficiency η) of $Cu_2ZnSn(S_{0.45}Se_{0.55})_4$ monograin layer solar cells made from non-etched and etched absorber crystals [27]*

Etchant	V_{oc} (mV)	J_{sc} (mA cm^{-2})	FF (%)	η (%)
None	300	10	40	1.2
Conc. HCl	342	11.5	48	1.9
2M NH_4OH	422	10.5	44	1.9
1% Br_2-MeOH	563	8.5	54	2.6
10% KCN	490	13.5	49	3.2
1% Br_2-MeOH +10% KCN	575	13.75	55	4.3

It can be seen that etching of the powder crystals improves the parameters of monograin layer solar cells. The combined chemical etching (1% Br_2-MeOH followed by etching with 10% KCN) of absorber material resulted in the highest values of solar cell parameters with efficiencies of approximately 4%. Higher efficiencies were obtained after further optimized surface thermal treatments.

13.4 Thermal Treatment of CZTS-Based Monograins

In general, monograin growth does not ensure an optimal absorber surface for solar cell formation. In addition to surface treatments by chemical etching, the composition of monograin surface could be adjusted by additional thermal treatments. The thermal process is more easily controlled by the temperature and atmosphere of treatment than the chemical etching.

High temperatures of up to 740°C are ordinarily used for thermal treatments of kesterites but, as reported earlier by different authors [30–32], kesterites start to decompose at temperatures of about 400°C. In order to prevent decomposition of the material, we needed to apply external vapor pressure in closed ampoules. In our experiments all post-treatments were carried out using two temperature zone arrangements. The temperatures of both zones were regulated and controlled independently. This allows more precise control of the vapor pressure during annealing.

13.4.1 $Cu_2ZnSnSe_4$

$SnSe_2$ or Se sources were used to regulate composition of the gas phase over $Cu_2ZnSnSe_4$ monograin powders. The following reactions describe the decomposition of $Cu_2ZnSnSe_4$ (Equation (13.1)) [31] and the formation of the gas phase (Equations (13.2)—(13.4)) at higher temperatures [33].

As a separate source, $SnSe_2$ decomposes according to the reactions described by Equations (13.2) and (13.3), providing SnSe and Se into the gas phase. Elemental selenium in a saturated gas phase consists of oligomers $Se_n(g)$, where $n = 2, 3, 5–8$ in the proportions that depend on the temperature [34].

$$Cu_2ZnSnSe_4(s) \leftrightarrow Cu_2Se(s) + ZnSe(s) + SnSe_2(s) \tag{13.1}$$

$$SnSe_2(s) \leftrightarrow SnSe(s) + 1/n\,Se_n(g); \quad K_p = P_{Sen}{}^{1/n} \tag{13.2}$$

$$SnSe(s) \leftrightarrow SnSe(g); \quad K_{SnSe} = P_{SnSe} \tag{13.3}$$

$$Cu_2ZnSnSe_4(s) \leftrightarrow Cu_2Se(s) + ZnSe(s) + SnSe(g) + 1/n\,Se_n(g); K_{CZTSe} = P_{SnSe} \times P_{Sen}{}^{1/n} \tag{13.4}$$

where K is the equilibrium constant and P is the partial pressure of the component.

Mass-spectrometric analysis [34] revealed that the vapor phase over solid SnSe consists mainly of SnSe vapor molecules as described by Equation (13.3), and that the equilibrium vapor pressure of pure SnSe is more than 4 orders of magnitude lower than the vapor pressure of pure $SnSe_2$ or Se. It is estimated from Equation 13.4 in chemical equilibrium that the reaction is shifted to the left side if $\log P_{Sen} > 1/n\,(\log K_{CZTSe} - \log P_{SnSe})$ and the incorporation of Sn from the gas phase of $SnSe_2$ into the $Cu_2ZnSnSe_4$ takes place. When the applied vapor pressure of Se is lower than the equilibrium vapor pressure, the decomposition of $Cu_2ZnSnSe_4$ is to an extent determined by the applied Se pressure.

Monograin powders with a large deviation of compositional ratios ($0.79<Cu/(Zn+Sn)<0.95$ and $0.93<Zn/Sn<1.2$) were used to study the influence of CZTSe thermal treatments on the performance of MGL solar cells [35]. During the annealing, the

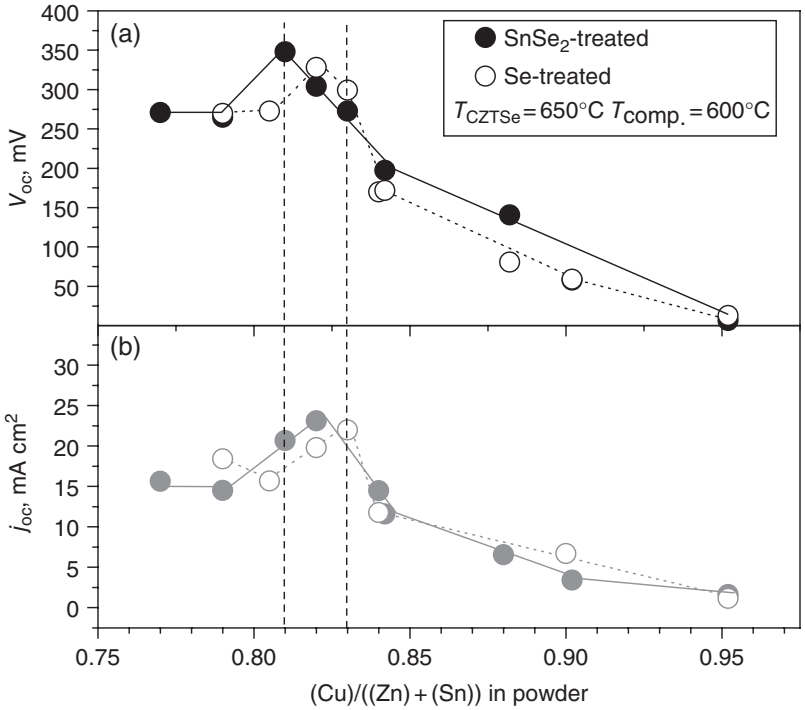

Figure 13.8 *Values of (a) short-circuit current density J_{sc} and (b) open-circuit voltage V_{oc} of CZTSe MGL solar cells as a function of [Cu]/([Zn]+[Sn]) ratio in the powder*

temperature in the material zone was 650°C and the temperature of the component zone ($SnSe_2$ or Se) was 600°C. The results (Fig. 13.8) showed that the values of V_{oc} depend on the Cu/(Zn+Sn) and Zn/Sn concentration ratios in the powder. The highest value V_{oc} = 350 mV was attained with the use of Cu-poor (Cu/(Zn+Sn) = 0.81–0.83) and Zn-rich (Zn/Sn = 1.1) powders. The measured value of J_{sc} = 23.8 mA cm^{-2} was also the highest in a limited range of Cu/(Zn+Sn) ratios. The solar cell characteristics were very low when the Cu-rich powders with the composition of Cu/(Zn+Sn) > 0.85 were used. An increase in the Cu content in powders resulted in a decrease in the Zn/Sn concentration ratio and $Cu_2ZnSnSe_4$ powders were of Sn-rich (Zn/Sn<1) composition.

The highest CZTSe-based solar cell efficiency (4.4%) was achieved with $SnSe_2$-annealed monograin powders with the composition Cu/(Zn+Sn) = 0.81 and Zn/Sn = 1.12 [35].

13.4.2 Cu_2ZnSnS_4

For sulphurization studies, the powders had Cu-poor ((Cu/(Zn+Sn) = 0.89)) and Zn-rich (Zn/Sn = 1.1) composition. EDX analysis confirmed that there was no change in the bulk composition of materials during the annealing in S or SnS_2 vapor [36]. By changing the parameters of sulfurization, optimal conditions for an effective absorber material were found. Detailed description of annealing parameters is provided in the literature [36].

Parameters of MGL solar cells consisting of S- or SnS_2-annealed absorbers were significantly affected by annealing temperatures. Efficiencies of Cu_2ZnSnS_4 MGL solar cells increased continuously with increasing material zone temperature from 550 to 740°C

(at sulfur pressure >100 Torr). These MGL solar cells show values of V_{oc} up to 690 mV and FF of up to 62%. Further increase in the sulfur vapor pressure did not lead to improvements of the solar cell parameters. When the vapor pressure of sulfur was <100 Torr, the precipitation of SnS_2 on the walls of the ampoules was visible. This means that relatively low S vapor pressure (P_S < 100 Torr) did not prevent Sn loss from Cu_2ZnSnS_4 and hence the decomposition of the surface region. A decomposed surface is not favorable for the formation of a working pn-junction, and our results confirm the statement of Wang *et al*. [37]. The highest values of J_{sc} = 18.4 mA cm^{-2} and V_{oc} = 768 mV were obtained using the Cu_2ZnSnS_4 powder that was annealed at 740°C in SnS_2 vapor. This value of V_{oc} was close to the highest value ever reported for Cu_2ZnSnS_4 [38]. Due to the use of epoxy, the active area and total area in MGL solar cells do not match. To evaluate the performance of separate monograins, a single-grain solar cell was constructed. The active area (1.05 mm^2) of the measured single monograin was determined by using the light-beam-induced current (LBIC) experiment. The open area of grain on the optical image (Fig. 13.9a) and active

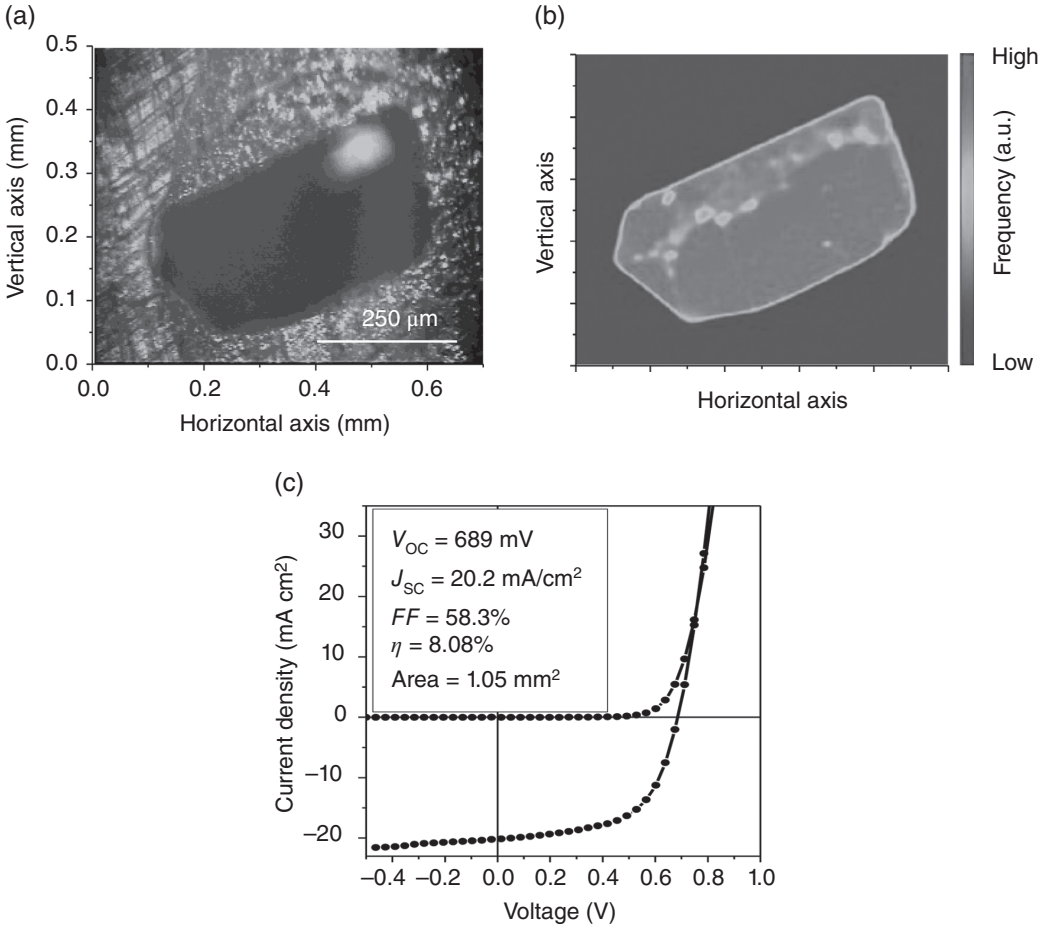

Figure 13.9 *(a) Optical image; (b) LBIC photoresponse map; and (c)* I–V *characteristics of CZTS single-grain solar cell. For color details, please see color plate section*

area on the LBIC image (Fig. 13.9b) are equal. Therefore, the performance of CZTS monograin powder material is 8.08% with the values of V_{oc} = 689 mV, J_{sc} = 20.2 mA cm^{-2}, and FF = 58.2% (Fig. 13.9c).

13.5 Optoelectronic Properties of CZTS-Based Monograins and Polycrystals

The optoelectronic properties of semiconductor materials are mainly determined by native and foreign defects. One prerequisite for obtaining high-efficiency solar cells is therefore to control the defect structure of the absorber material. Theoretical first-principles calculations [39, 40] predict low-defect-formation energies of the order a few hundred milli-electron volts for many isolated point defects as well as defect complexes in CZTS and CZTSe, meaning that control over the defect structure of these compounds is rather complicated. We studied defects in CZTS and CZTSe monograins and polycrystals using mainly photoluminescence (PL) spectroscopy. Admittance spectroscopy (AS) was used for the determination of deep levels in the corresponding MGL solar cells.

In good-quality CZTS crystals and CZTSe thin films, excitonic emission together with a PL emission involving shallow defect levels have been detected [41, 42]. However, the PL spectra of both CZTS and CZTSe monograins at T = 10 K consist of broad (full-width at half-maximum or FWHM being more than 100 meV) asymmetric PL bands (Fig. 13.10) [43–45]. An asymmetric shape of the PL bands and a large blue-shift of the order more than 10 meV/decade with increasing laser power are commonly seen in heavily doped and

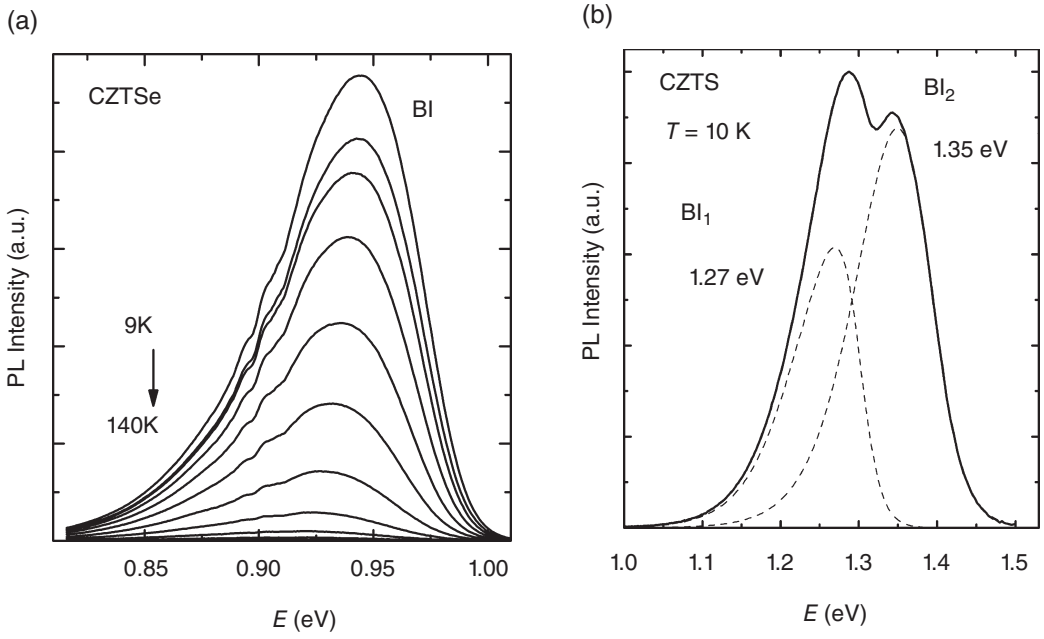

Figure 13.10 *(a) Temperature dependence of the PL spectra of CZTSe monograins; and (b) low-temperature PL spectrum of CZTS polycrystals together with the fitting result. Reproduced from [44] and [45], respectively. With permission from Elsevier*

compensated semiconductors where spatial potential fluctuations are present [46–49]. The conditions of heavy doping in the present case originate from the high concentration of native defects that is often observed in multinary semiconductor compounds. The spatial potential fluctuations lead to a local perturbation of the band structure, giving rise to broadened defect energy levels and also band tails. In a p-type material and in the case of small effective mass of electrons, radiative recombination can therefore mainly arise from four different channels [46]: band-to-tail recombination (BT) that is associated with a free electron and a hole which is localized in the valence band tail; band-to-band recombination (BB) that involves a free electron and a free hole; band-to-impurity (BI) recombination that involves an acceptor state that is deep enough not to overlap with the valence band tail; and donor–acceptor pair (DAP) recombination that involves an acceptor and a donor state that are deep enough not to overlap with the corresponding band tails.

For comparison, PL and Raman scattering of CZTS polycrystalline powders and monograins were studied. It was found that, in some cases, much narrower PL bands and Raman peaks measured from the polycrystalline powders enabled a better description of the recombination processes and vibrational properties of CZTS.

PL analysis of the CZTSe monograins indicates that the dominant recombination mechanism at low temperatures is BI recombination [44]. The BI-type PL band in CZTSe was found at 0.95 eV at $T = 10$ K (see Fig. 13.10a) and could be attributed to acceptor defects with ionization energy of $E_T = 69 \pm 4$ meV [44].

In polycrystalline CZTS, two PL bands were observed at 1.27 eV and 1.35 eV at $T = 10$ K, as shown in Figure 13.10b. Both PL bands showed similar dependence on temperature and excitation power corresponding to BI recombination [45]. Interestingly, similar thermal activation energies around 280 meV were determined from the temperature dependence of these PL bands in CZTS. Considering the Raman scattering results of the polycrystalline powder, we proposed that the observed PL bands arise from the BI recombination process involving the same deep acceptor defect with ionization energy of around 280 meV, but different CZTS phase (kesterite and disordered kesterite) with different band-gap energy [45].

Very narrow Raman peaks of CZTS polycrystals (FWHM of the A_1 peak was 2.6 cm^{-1}; see Fig. 13.11) enabled us to detect the co-existence of two polytypes in CZTS: the kesterite and the disordered kesterite phase [45]. The general consensus is that the kesterite structure is the ground-state structure but, according to the theoretical calculations [50], the formation energy difference between the different polytypes is only of the order of a few millielectron volts per atom, indicating that the disorder in the cation sublattice may occur under standard growth conditions. The disorder is predicted to cause a band-gap energy difference of around 0.1 eV for the kesterite and the disordered kesterite or stannite phase in CZTS, the kesterite having the largest band-gap energy [50]. Neutron diffraction measurements [51, 52] also showed that a partially disordered kesterite structure exists. Although the vibrational spectra of these phases are also similar, according to theoretical calculations [53, 54] there is a difference at least in A_1 phonon modes of kesterite, disordered kesterite, and stannite CZTS. Since such narrow Raman peaks are usually not seen, they are not resolved; however, the coexistence of the different polytypes should always be considered.

In addition to the BI recombination involving deep acceptor defect, there is another recombination mechanism possible in CZTS resulting in the PL emission at the same

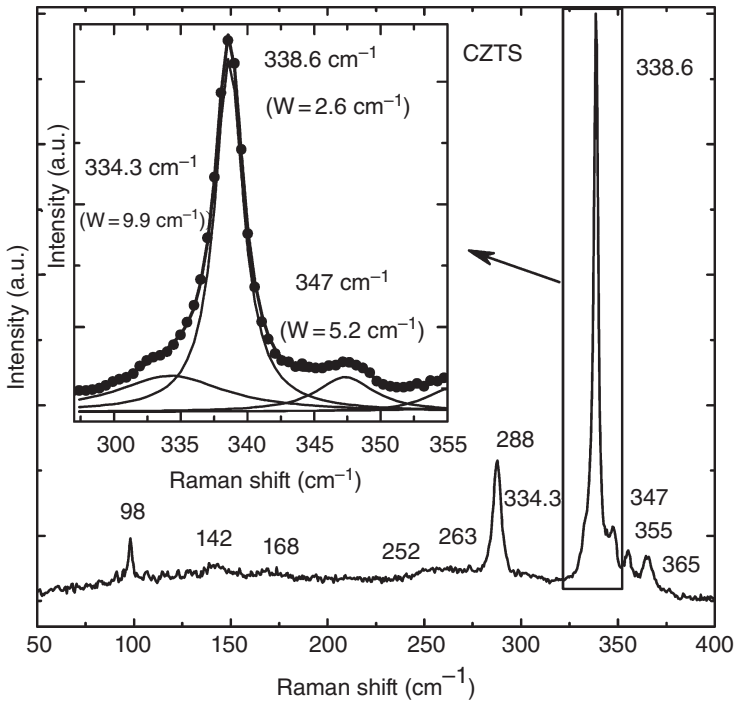

Figure 13.11 *Raman spectrum of CZTS polycrystals. The fitting result for the A_1 peak is shown on the inset graph, where the original spectrum is represented by symbols. A shoulder peak corresponding to A_1 mode of disordered kesterite phase is observed at 334.3 cm^{-1} [45]*

energy of around 1.3 eV, but lower thermal quenching activation energy of about 100 meV. Our low-temperature PL measurements of near-stoichiometric CZTS monograins and polycrystals revealed a very deep PL band at 0.66 eV (PL1) together with the 1.35 eV emission (PL2) (see Fig. 13.12a) [55]. The dominant radiative recombination mechanism in this case is the recombination between electrons and holes in the quantum well caused by the $(2Cu_{Zn}^{-} + Sn_{Zn}^{2+})$ defect clusters that induce a significant band-gap decrease of 0.35 eV, as shown in [40]. As a result, the PL2 band at 1.35 eV arises. At low temperatures BI recombination involving deep donor level is also present, giving the PL1 band with the peak position of 0.66 eV. We propose that it originates from the partially compensated $(Cu_{Zn}^{-} + Sn_{Zn}^{2+})$ defect cluster. According to the theoretical calculations [40], the donor level is situated at c. 0.63 eV below the conduction band minimum (the recombination model is presented in Fig. 13.12b). Theoretical calculations [40] predict a high concentration of $(2Cu_{Zn}^{-} + Sn_{Zn}^{2+})$ and $(Cu_{Zn}^{-} + Sn_{Zn}^{2+})$ defect clusters in nearly stoichiometric CZTS. Other types of defect clusters were also predicted in CZTS [56]. These defect clusters will either produce deep recombination centers for electron–hole pairs or cause trapping of charge carriers. Both mechanisms are detrimental to solar cell parameters and should be avoided. Interestingly, it is predicted [40] that the detrimental effect of both defect clusters is weaker in CZTSe since the donor levels induced by Sn_{Zn} are shallower in CZTSe than in CZTS. To date, there is no experimental evidence of the presence of these defect clusters in CZTSe.

At lower temperatures, BI or quantum well types of recombination alway dominate in CZTS monograins and polycrystalline powders. BT emission, which is very common for

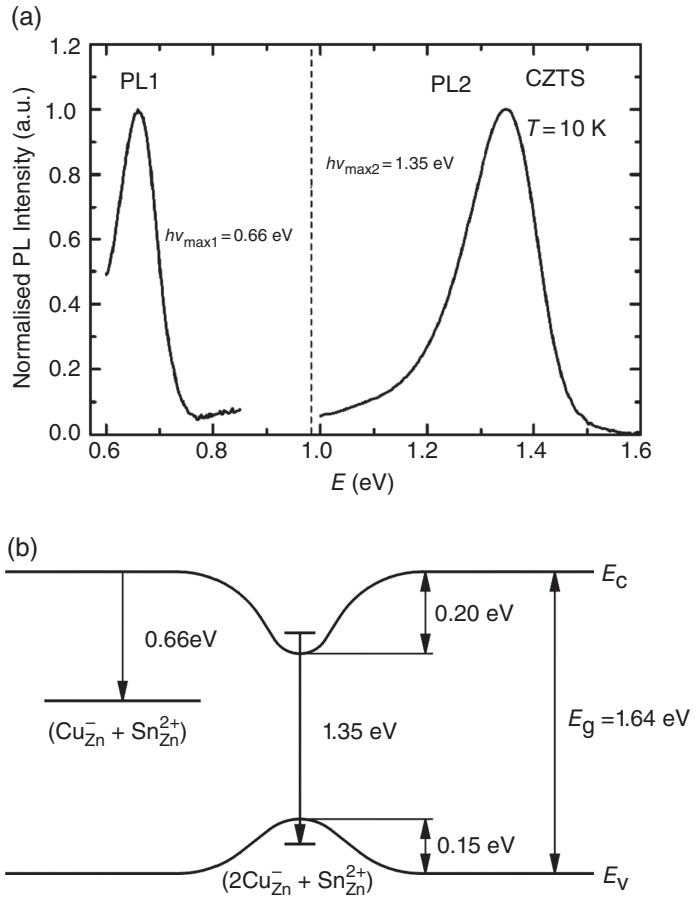

Figure 13.12 *(a) Low-temperature (T=10 K) PL spectrum of near-stoichiometric CZTS; and (b) the corresponding radiative recombination model. Reproduced from [55]. With permission from Elsevier*

other heavily doped multinary compounds, has very low intensity in CZTS and can be detected at 1.39 eV (and the BB band at 1.53 eV) at high temperatures only, when the BI or quantum well type of recombinations are quenched, and at a high excitation level (see Fig. 13.13) [57]. The results of our RT micro-PL experiments at high excitation level confirm that the model of heavily doped semiconductors [46] also applies to CZTS.

Deep defect levels in CZTS and CZTSe MGL solar cells have also been studied by admittance spectroscopy (AS) [58, 59]. We found two deep defect states in both materials from temperature-dependent AS measurements (Table 13.3; Fig. 13.14a). The first state (E_{A1}) was present in different CZTS and CZTSe cells, while the second state (E_{A2}) had somewhat different properties in different cells. The activation energy of the latter defect state varied in different cells and was dependent on the applied bias voltage (0 V, –1 V), which is uncommon for bulk defect states. The first state is therefore attributed to an acceptor level and the second to the interface states. The corresponding activation energies are presented in Table 13.3. The activation energies of the acceptor defects are in agreement with the values obtained from the PL analysis of the corresponding CZTS and CZTSe monograins.

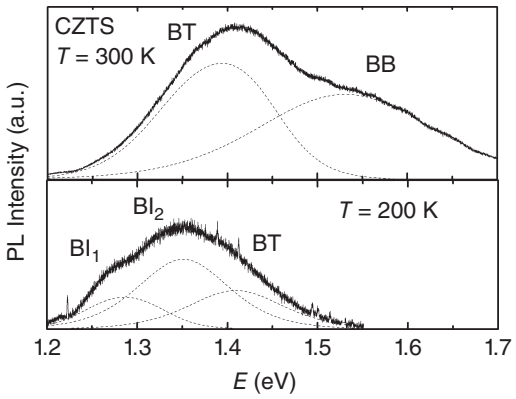

Figure 13.13 *Micro-PL spectra of CZTS. Reproduced with permission from [57]. SPIE*

Table 13.3 *Activation energies found by AS of the measured heterojunctions. Results for an aged device are in brackets.* E_{A2} *is attributed to the interface states and* E_{A1} *to acceptor defects [52, 53]*

Material	E_{A1} (meV)	E_{A2} (meV)
$Cu_2ZnSnSe_4$	75±2 (74±2)	87±3 (100±3)
$Cu_2ZnSn(Se_{0.75}S_{0.25})_4$	25±5	154±7
Cu_2ZnSnS_4	120±1	167±8

We have also studied the temperature dependence of the output parameters of the $Cu_2ZnSn(Se_{0.3}S_{0.7})_4$ monograin layer solar cells [60]. We found that for a light intensity of 100 mW cm^{-2}, dV_{oc}/dT = –1.91 mV K^{-1}. Especially important is the temperature dependence of the relative efficiency η of solar cells (Fig. 13.14b). Calculated efficiencies are not calibrated because a halogen light source was used and therefore AM1.5 spectral conditions were not followed. It can be seen that the efficiencies have a maximum value below room temperature. The corresponding maximum efficiency temperature increases with light intensity and at 100 mW cm^{-2} is at about 250 K. At low temperatures, efficiency starts to diminish with decreasing temperature. The same behavior can also be observed at temperatures above 250 K. In the higher temperature region, the decrease of efficiency is nearly linear with temperature. For a standard light intensity, the relative efficiency of the solar cell decreases with the temperature at a slope of 0.013% K^{-1}.

Measured temperature coefficients of CZTSSe MGL solar cells indicate that in many cases they are lower than for other types of solar cells. For example, $Cu(In,Ga)Se_2$ cells usually show dV_{oc}/dT values from –2.01 to –3.3 mV K^{-1} and $d\eta/dT$ values from –0.017 to –0.064% K^{-1} [61]. Si cells show dV_{oc}/dT values from –2.07 to –2.17 mV K^{-1} and a $d\eta/dT$ value of about –0.042% K^{-1} [62]. The same applies to the situation in CdTe cells, where dV_{oc}/dT is typically in the range of –2.1 to –2.2 mV K^{-1} [63]. These low values of measured temperature coefficients of CZTSSe solar cells show a great potential for this compound.

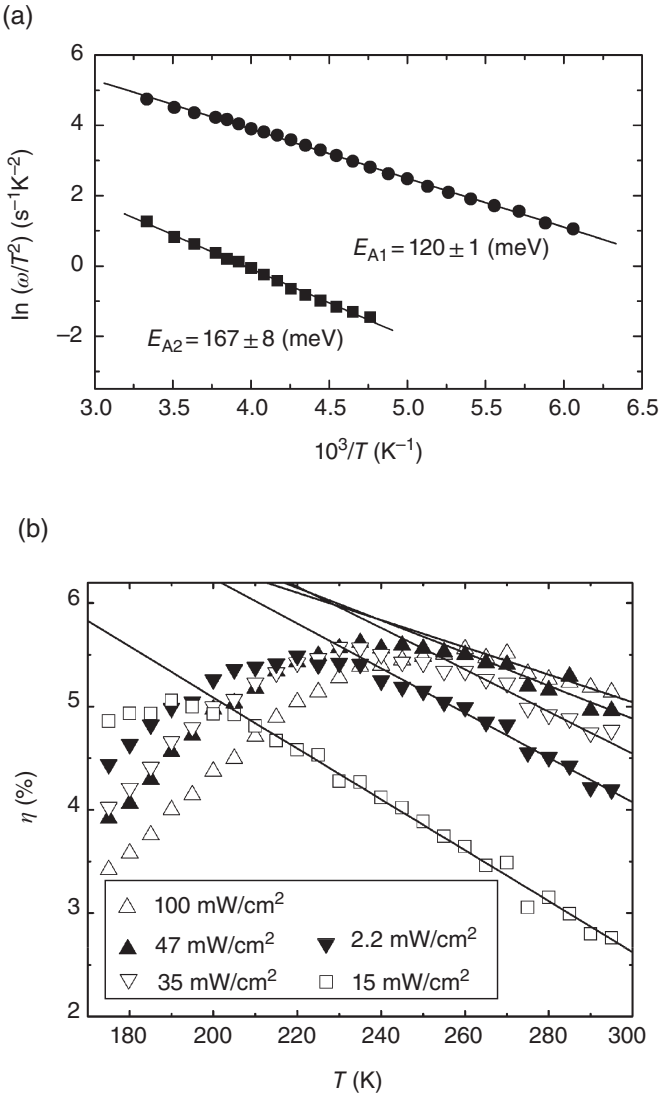

Figure 13.14 *(a) Arrhenius plot showing the calculated activation energies of the defect levels in CZTS. The measurements are performed at bias 0 V. (b) Temperature dependence of the relative efficiency η of a CZTSSe MGL solar cell under different light intensities. Reproduced from [58] and [60], respectively. With permission from Elsevier*

13.6 Conclusion

In conclusion, we have shown that monograin powder technology is one of the methods for the growth of high-quality CZTSSe absorber materials for solar cells. In the growth of kesterite-type monograin powders, the crystals are formed in the presence of the liquid phase of water-soluble flux salts (KI, NaI, CdI_2) that increases the homogeneity of the product absorber material and control the particle size and shape as well as their agglomeration state. The method enables the growth of different solid solutions

$Cu_2ZnSn(S_{1-x}Se_x)_4$, $Cu_2(Zn_xCd_{1-x})SnS_4$, $Cu_2Zn(Sn_xGe_{1-x})Se_4$. In the monograin-layer solar cell structure graphite/CZTS/CdS/ZnO, the CZTS has shown the highest solar energy conversion efficiency of 8.1% (V_{oc} = 768 mV, FF = 69%, J_{sc} = 20.2 mA cm^{-2}). The optical and physical investigations have shown that the kesterite-type absorber materials include a high concentration of native defects that give rise to a strong recombination in the bulk of the absorber. The observed radiative recombination involves deep acceptor defects acting as carrier traps, or defect clusters which decrease the band-gap energy of the material. Strong recombination in the bulk of the absorber and the interface recombination in the solar cells are responsible for current and voltage losses in the kesterite-based solar cells.

References

[1] Chapin, D.M., Fuller, C.S. & Pearson, G.L. (1954) A new silicon *p-n* junction photocell for converting solar radiation into electrical power. *Journal of Applied Physics*, **25**, 676–677.

[2] Paradise, M.E. (1957) Large area solar energy converter and method for making the same. US Patent 2,904,613, August 26.

[3] Ties Siebolt Te Velde (1965) Electrical monograin layers having a radiation permeable electrode. US3480818 A, August 4.

[4] Kilby, J.S., Lathrop, J.W. & Porter, W.A. (1977) Solar enery conversion. US4021323A, May 3.

[5] Taira, K. & Nakata, J. (2010) Silicon cells: catching rays. *Nature Photonics*, **4**, 602–603.

[6] Meissner, D. (2013) Photovoltaics based on semiconductor powders. In: *Materials and Processes for Energy: Communicating Current Research and Technological Developments* (ed. A. Méndez-Vilas), Formatex Research Center Badajoz, Spain.

[7] Sundermeyer, W. (1963) Fused salts and their use as reaction media. *Angewandte Chemie, International Edition*, **4**, 222–238.

[8] Kerridge, D.H. (1975) Recent advances in molten salts as reaction media. *Pure and Applied Chemistry*, **41**, 355–371.

[9] Arendt, R.H. (1973) The molten salt synthesis of single magnetic domain $BaFe_{12}O_{19}$ and $SrFe_{12}O_{19}$ crystals. *Journal of Solid State Chemistry*, **8**, 339–347.

[10] Boistelle, R. & Astier, J.P. (1988) Crystallization mechanisms in solution. *Journal of Crystal Growth*, **90**, 14–30.

[11] Mellikov, E., Hiie, J. & Altosaar, M. (2007) Powder materials and technologies for solar cells. *International Journal of Materials and Product Technology*, **28**, 291.

[12] Altosaar, M., Hiie, J., Mellikov, E. & Mädasson, J. (1996) Recrystallyzation of CIS powders in molten fluxes. *Crystal Research and Technology*, **31**, 505–508.

[13] Hiie, J., Altosaar, M. & Mellikov, E. (1999) Comparative study of isothermal grain growth of CdS and CdTe in the presence of halide fluxes. *Solid State Phenomena*, **67–68**, 303–308.

[14] Altosaar, M. & Mellikov, E. (1999) $CuInSe_2$ monograin growth in CuSe-Se liquid phase. *Japanese Journal of Applied Physics*, **39**, 65–66.

[15] Hiie, J., Altosaar, M., Mellikov, E., Kukk, P., Sapogova, J. & Meissner, D. (1999) growth of CdTe monograin powders. *Physica Scripta*, **T69**, 155–158.

[16] Hiie, J., Altosaar, M., Mellikov, E., Mikli, V., Mädasson, J. & Sapogova, J. (1997) Isothermal grain growth of CdTe in $CdCl_2$ and Te fluxes. In: *Conference Records of the 26th IEEE Photovoltaic Specialists Conference. IEEE Operations Center*, 455–458.

[17] Timmo, K., Altosaar, M., Kauk, M., Raudoja, J. & Mellikov, E. (2007) $CuInSe_2$ monograin growth in the liquid phase of potassium iodide. *Thin Solid Films*, **515**, 5884–5886.

[18] Altosaar, M., Raudoja, J., Timmo, K., Danilson, M., Krunks, M. & Mellikov, E. (2006) $Cu_2ZnSnSe_4$ monograin powders for solar cell application. In: *Conference Record of the 2006 IEEE 4th World Conference on Photovoltaic Energy Conversion.* Waikoloa, HI, May 07–12. IEEE Electron Devices Society, 468–470.

[19] Altosaar, M., Raudoja, J., Timmo, K., Danilson, M., Grossberg, M., Krustok, J. & Mellikov, E. (2008) $Cu_2Zn_{1-x}Cd_xSn(Se_{1-y}S_y)_4$ solid solutions as absorber materials for solar cells. *Physica Status Solidi A*, **205**, 167–170.

[20] Leinemann, I., Raudoja, J., Grossberg, M., Traksmaa, R., Kaljuvee, T., Altosaar, M. Meissner, D. (2010) Comparison of copper zinc tin selenide formation in molten potassium iodide and sodium iodide as flux materials. In: *Proceedings of the Conference of Young Scientists on Energy Issues*, Kaunas, Lithuania 2010, 1–8.

[21] Klavina, I., Kaljuvee, T., Timmo, K., Raudoja, J., Traksmaa, R., Altosaar, M. & Meissner, D. (2011) Study of $Cu_2ZnSnSe_4$ monograin formation in molten KI starting from binary chalcogenides. *Thin Solid Films*, **519**, 7399–7407.

[22] Nkwusi, G., Leinemann, I., Grossberg, M., Kaljuvee, T., Traksmaa, R., Altosaar, M. & Meissner, D. (2012) Formation of copper zinc tin sulfide in cadmium iodide for monograin membrane solar cells. In: *Proceedings of the 9th International Conference of Young Scientists on Energy Issues*, Kaunas, May 24–25 2012, 38–46.

[23] Chen, S., Gong, X.G., Walsh, A. & Wei, S.H. (2010) Defect physics of the kesterite thin-film solar cell absorber Cu_2ZnSnS_4. *Applied Physics Letters*, **96**, 021902.

[24] Muska, K., Kauk, M., Altosaar, M., Pilvet, M., Grossberg, M. & Volobujeva, O. (2011) Synthesis of Cu_2ZnSnS_4 monograin powders with different compositions. *Energy Procedia,* **10**, 203–207.

[25] Muska, K., Kauk, M., Grossberg, M., Raudoja, J. & Volobujeva, O. (2011) Influence of compositional deviations on the properties of $Cu_2ZnSnSe_4$ monograin powders. *Energy Procedia*, **10**, 323–327.

[26] Olekseyuk, I.D., Dudchak, I.V. & Piskach, L.V. (2004) Phase equilibria in the Cu_2S–ZnS–SnS_2 system. *Journal of Alloys and Compounds*, **368**, 135–143.

[27] Timmo, K., Altosaar, M., Raudoja, J., Grossberg, M., Danilson, M., Volobujeva, O. & Mellikov, E. (2010) Chemical etching of $Cu_2ZnSn(S,Se)_4$ monograin powder. In: *Proceedings of 35th IEEE Photovoltaic Specialists Conference*, Honolulu, HI, June 20–25 2010, 1982–1985.

[28] Pourbaix, M. (1974) *Atlas of Electrochemical Equilibria in Aqueous Solutions II*. National Association of Corrosion Engineers, Houston, US.

[29] Scheer, R., Walter, T., Schock, H.W., Fearheiley, M.L. & Lewerenz, H.J. (1993) $CuInS_2$ based thin film solar cell with 10.2% efficiency. *Applied Physics Letters*, **63**, 3294–3296.

[30] Weber, A., Mainz, R. & Schock, H.W. (2010) On the Sn loss from thin films of the material system Cu–Zn–Sn–S in high vacuum. *Journal of Applied Physics*, **107**, 013516.

[31] Scragg, J., Ericson, T., Kubart, T., Edoff, M. & Platzer-Björkman, C. (2011) Chemical insights into the instability of Cu_2ZnSnS_4 films during annealing. *Chemistry of Materials*, **23**, 4625–4633.

[32] Redinger, A., Berg, D.M., Dale, P.J., Djemour, R., Gütay, L., Eisenbarth, T., Valle, N. & Siebentritt, S. (2011) Route toward high-efficiency single-phase $Cu_2ZnSn(S,Se)_4$ thin-film solar cells: model experiments and literature review. *IEEE Journal of Photovoltaics*, **1**, 200–206.

[33] Gerasimov, J.I., Krestovnikov, A. & Gorbov, V. (1974) *Chimitsheskaja termodinamika v cvetnoi metallurgii*. Metallurgia, Moscow (in Russian).

[34] Brebrick, R.F. & Strauss, A.J. (1964) Partial pressures in equilibrium with group IV tellurides I, Optical absorption method and results for PbTe. *Journal of Chemical Physics*, **40**, 3230–3241.

[35] Kauk-Kuusik, M., Altosaar, M., Muska, K., Pilvet, M., Raudoja, J., Timmo, K., Varema, T., Grossberg, M., Mellikov, E. & Volobujeva, O. (2013) Post-growth annealing effect on the performance of $Cu_2ZnSnSe_4$ monograin layer solar cells. *Thin Solid Films*, **535**, 18–21.

[36] Kauk, M., Muska, K., Altosaar, M., Raudoja, J., Pilvet, M., Varema, T., Timmo, K. & Volobujeva, O. (2011) Effects of sulphur and tin disulphide vapour treatments of $Cu_2ZnSnS(Se)_4$ absorber materials for monograin solar cells. *Energy Procedia*, **10**, 197–202.

[37] Wang, K., Shin, B., Reuter, K.B., Todorov, T., Mitzi, D.B. & Guha, S. (2011) Structural and elemental characterization of high efficiency Cu_2ZnSnS_4 solar cells. *Applied Physics Letters*, **98**, 051912.

[38] Katagiri, H., Ishigaki, N., Ishida, T. & Saito, K. (2001) Characterization of Cu_2ZnSnS_4 thin films prepared by vapor phase sulfurization. *Japanese Journal of Applied Physics*, **40**, 500–504.

[39] Chen, S., Yang, J.H., Gong, X.G., Walsh, A. & Wei, S.H. (2010) Intrinsic point defects and complexes in the quaternary kesterite semiconductor Cu_2ZnSnS_4. *Physics Reviews B*, **81**, 245204.
[40] Chen, S., Wang, L.W., Walsh, A., Gong, X.G. & Wei, S.H. (2012) Abundance of Cu_{Zn}+Sn_{Zn} and $2Cu_{Zn}$+Sn_{Zn} defect clusters in kesterite solar cells. *Applied Physics Letters*, **101**, 223901.
[41] Hönes, K., Zscherpel, E., Scragg, J. & Siebentritt, S. (2009) Shallow defects in Cu_2ZnSnS_4. *Physica B: Condensed Matter*, **404**, 4949–4952.
[42] Luckert, F., Hamilton, D.I., Yakushev, M.V., Beattie, N.S., Zoppi, G., Moynihan, M., Forbes, I., Karotki, A.V., Mudryi, A.V., Grossberg, M., Krustok, J. & Martin, R.W. (2011) Optical properties of high quality $Cu_2ZnSnSe_4$ thin films. *Applied Physics Letters*, **99**, 062104.
[43] Grossberg, M., Krustok, J., Raudoja, J., Timmo, K., Altosaar, M. & Raadik, T. (2011) Photoluminescence and Raman study of $Cu_2ZnSn(Se_xS_{1-x})_4$ monograins for photovoltaic applications. *Thin Solid Films*, **519**, 7403–7406.
[44] Grossberg, M., Krustok, J., Timmo, K. & Altosaar, M. (2009) Radiative recombination in $Cu_2ZnSnSe_4$ monograins studied by photoluminescence spectroscopy. *Thin Solid Films*, **517**, 2489–2492.
[45] Grossberg, M., Krustok, J., Raudoja, J. & Raadik, T. (2012) The role of structural properties on deep defect states in Cu_2ZnSnS_4 studied by photoluminescence spectroscopy. *Applied Physics Letters*, **101**, 102102.
[46] Levanyuk, A.P. & Osipov, V.V. (1981) Edge luminescence of direct-gap semiconductors. *Soviet Physik Uspekhi*, **24**, 187–215.
[47] Krustok, J., Jagomägi, A., Grossberg, M., Raudoja, J. & Danilson, M. (2006) Photoluminescence properties of polycrystalline $AgGaTe_2$. *Solar Energy Materials and Solar Cells*, **90**, 1973–1982.
[48] Krustok, J., Collan, H., Yakushev, M. & Hjelt, K. (1999) The role of spatial potential fluctuations in the shape of the PL bands of multinary semiconductor compounds. *Physica Scripta,* **T79**, 179–182.
[49] Krustok, J., Raudoja, J., Yakushev, M., Pilkington, R.D. & Collan, H. (1999) On the shape of the close-to-band-edge photoluminescent emission spectrum in compensated $CuGaSe_2$. *Physica Status Solidi (A)*, **173**, 483–490.
[50] Chen, S., Gong, X.G., Walsh, A. & Wei, S.H. (2009) Crystal and electronic band structure of Cu_2ZnSnX_4 (X=S and Se) photovoltaic absorbers: First-principles insights. *Applied Physics Letters*, **94**, 041903.
[51] Schorr, S., Hoebler, H.J. & Tovar, M. (2007) A neutron diffraction study of the stannite-kesterite solid solution series. *European Journal of Mineralogy*, **19**, 65–73.
[52] Schorr, S. (2011) The crystal structure of kesterite type compounds: A neutron and X-ray diffraction study. *Solar Energy Materials and Solar Cells*, **95**, 1482–1488.
[53] Gürel, T., Sevik, C. & Cagin, T. (2011) Characterization of vibrational and mechanical properties of quaternary compounds Cu_2ZnSnS_4 and $Cu_2ZnSnSe_4$ in kesterite and stannite structures. *Physics Reviews B*, **84**, 205201.
[54] Khare, A., Himmetoglu, B., Johnson, M., Norris, D.J., Cococcioni, M. & Aydil, E.S. (2012) Calculation of the lattice dynamics and Raman spectra of copper zinc tin chalcogenides and comparison to experiments. *Journal of Applied Physics*, **111**, 083707.
[55] Grossberg, M., Raadik, T., Raudoja, J.. & Krustok, J. (2014) Photoluminescence study of defect clusters in Cu_2ZnSnS_4 polycrystals. *Current Applied Physics*, **14**, 447–450.
[56] Huang, D. & Persson, C. (2013) Band gap change induced by defect complexes in Cu_2ZnSnS_4. *Thin Solid Films*, **535**, 265–269.
[57] Grossberg, M., Salu, P., Raudoja, J. & Krustok, J. (2013) Microphotoluminescence study of Cu_2ZnSnS_4 polycrystals. *Journal of Photonics for Energy*, **3**, 030599.
[58] Kask, E., Raadik, T., Grossberg, M., Josepson, R. & Krustok, J. (2011) Deep defects in Cu_2ZnSnS_4 monograin solar cells. *Energy Procedia*, **10**, 261–265.
[59] Kask, E., Grossberg, M., Josepson, R., Salu, P., Timmo, K. & Krustok, J. (2013) Defect studies in $Cu_2ZnSnSe_4$ and $Cu_2ZnSn(Se_{0.75}S_{0.25})_4$ by admittance and photoluminescence spectroscopy. *Materials Science in Semiconductor Processing*, **16**, 992–996.
[60] Krustok, J., Josepson, R., Danilson, M. & Meissner, D. (2010) Temperature dependence of $Cu_2ZnSn(Se_xS_{1-x})_4$ monograin solar cells. *Solar Energy*, **84**, 379–383.

[61] Kniese, R., Hariskos, D., Voorwinden, G., Rau, U. & Powalla, M. (2003) High band gap Cu(In,Ga)Se_2 solar cells and modules prepared with in-line co-evaporation. *Thin Solid Films*, **431–432**, 543–547.
[62] Singh, P., Singh, S.N., Lal, M. & Husain, M. (2008) Temperature dependence of I-V characteristics and performance parameters of silicon solar cell. *Solar Energy Materials and Solar Cells*, **92**, 1611–1616.
[63] Phillips, J.E., Shafarman, W.N. & Shan, E. (1994) Evidence for amorphous like behavior in small grain thin film polycrystalline solar cells. In: *Proceedings of IEEE First WCPEC (24th IEEE PVSC)*, 303–306.